

The Power Factor Maximums of Alloy $\text{Si}_x\text{Ge}_{1-x}$ and Some Other Thermoelectric

ABSTRACT

In this article, the issue of determining the power factor maximums of $\text{Si}_x\text{Ge}_{1-x}$ alloy with different compositions is investigated. This issue is discussed also for other thermoelectrics based on literature data. It is shown that for the values of the Seebeck coefficient in the interval $(1-4)10^{-4}\text{V/K}$, $(\text{PF})_{\text{max}}$ corresponds to the minimum of the specific electrical conductivity. The interdependence of these thermoelectric parameters has a regular character. The dependences $\lg(\sigma\text{S}^2)_{\text{max}} - \lg\sigma_{\text{min}}$ for various thermoelectrics based on literature and our data in the corresponding interval of changes of variables are described by a single empirical expression $\lg(\sigma\text{S}^2)_{\text{max}} \cong 0.583(\lg\sigma_{\text{min}})^2 - 3.332\lg\sigma_{\text{min}}$. The temperature dependence of the Seebeck coefficient described by the equation $S = \frac{3k_B}{2q_e} \ln T + C$, where C depends on the concentration and effective mass of charge carriers, as well as on the Debye temperature. This dependence has the same character as dependence $\sigma\text{S}^2 - T$ and have maximum around 1100K. Additionally, the dependences of power factor on specific electrical conductivity were studied. For different thermoelectrics they are described by empirical expressions such as $\sigma\text{S}^2 \cong (a/\sigma) - b$ or $\sigma\text{S}^2 \cong c\sigma^{-d}$, where constants a, b, c and $d > 0$. For a number of thermoelectrics, the dependences σS^2 on the Seebeck coefficient are rectilinear, while for another series they are power-law. And this is a more general case. The temperature dependences of σS^2 and of scaled power factor (B_S) are also studied. Both are described by a quadratic equation. It has been established that the maximum power factor corresponds to the minimum B_S . Thus, in this case to estimate $(\sigma\text{S}^2)_{\text{max}}$ can be used as σ_{min} , and $(B_S)_{\text{min}}$.

Keywords: SiGe thermoelectric; power factor; electrical conductivity.

1. INTRODUCTION

Since the seventies of the last century, the $\text{Si}_x\text{Ge}_{1-x}$ alloy has been used in thermoelectric generators in spacecraft for long-distance flights with a long service life [1-3]. This alloy is also used in many branches of science and technology [4-15].

N-type $\text{Si}_x\text{Ge}_{1-x}$ has a number of advantages over the P-type: the maximum of figure of merit (ZT) is about 2.5 times greater for N-type than for P-type (at concentration of charge carriers $n = 3.2 \cdot 10^{26} \text{m}^{-3}$ and at the same compositions). This follows from the fact that the specific electrical conductivity is 2.5-3 times higher, Seebeck coefficient is 1.4-2 times larger (accordingly, the power factor is ~2 orders of magnitude greater), and thermal conductivity coefficient is 1.1-1.3 times smaller at the same temperatures. Also with neutron fluencies $\geq 10^{19}$ and irradiation temperatures $\geq 600^\circ\text{C}$ N-type $\text{Si}_x\text{Ge}_{1-x}$ is more radiation resistant [16].

This article is a continuation of work [17], where the maximization of the figure of merit of thermoelectric material SiGe is considered. Together with ZT, power factor (PF) is an important energy characteristic of thermoelectrics, which is included in the expression of the ZT: $PF \equiv \sigma S^2$, where σ is the specific electrical conductivity, S - Seebeck coefficient. Here was studied N-Si_xGe_{1-x} alloy at $x=0.7, 0.72, 0.76, 0.8$ and 0.83 . Experimental data taken from [18]. Since the remaining thermoelectric materials are also taken from the literature, the experimental section is not included.

Seebeck coefficient

According to a fairly large number of works, the range of changes of the Seebeck coefficient is $(1-4)10^4$ V/K. With such a relatively narrow range, the σS^2 - S dependence is almost rectilinear: $\sigma S^2 = kS + b$, where k is the slope of the straight lines, and b is the ordinate of the point of their intersection with the axis σS^2 when extrapolating these lines to $S \rightarrow 0$. From the last equation we get: $S = \frac{k}{2\sigma} + \left[\left(\frac{k}{2\sigma} \right)^2 + \frac{b}{\sigma} \right]^{1/2}$. After simple transformations we will have: $\sigma S^2 = \frac{k}{2\sigma} + b$, that is, in this case $(PF)_{\max}$ will correspond to σ_{\min} .

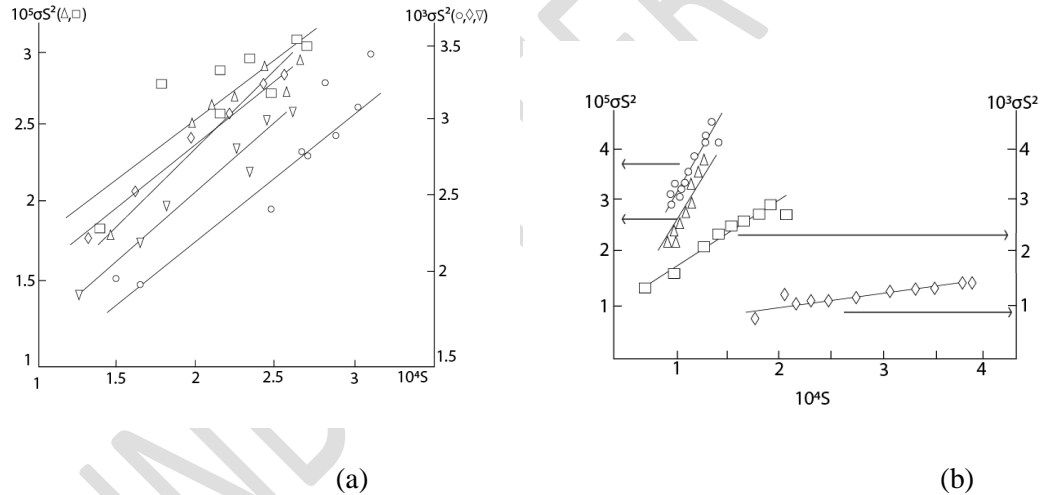


Fig. 1. Typical dependences σS^2 - S : (a) Si_xGe_{1-x}, $x=0.7$ (o), 0.72 (Δ), 0.76 (\square), 0.8 (\diamond) and 0.83 (∇); (b) (o) Bi₂Sr_{1.925}[Sr(BO₂)₂]_{0.075}Co_{1.8}O_y [18], (Δ) Bi₂Sr₂Co_{1.8}O_y [18], \square - SiGeMo_{0.2} [19], and (\diamond) Sb_{1.7}Bi_{0.4}Te₃ [20]. [σS^2]=W/K²m, [S]=V/K.

Thermoelectrics

Figure 2 shows $\lg(\sigma S^2)_{\max} - \lg\sigma_{\min}$ dependences for different thermoelectrics using literature and our data. In the obtained intervals of change of variables, these dependencies can be described as a whole by the empirical expression $\lg(\sigma S^2)_{\max} \cong 0.583(\lg\sigma_{\min})^2 - 3.332\lg\sigma_{\min}$ (solid line in Fig.2). The entire dependence is divided into three areas: (I) $10^{-2} < (PF)_{\max} < 10^{-3}$, (II) $10^{-3} < (PF)_{\max} < 10^{-4}$ and (III) $10^{-4} < (PF)_{\max} < 10^{-5}$.

$^5\text{W/K}^2\text{m}$. By means of this approximate relationship, it will be possible to predict the order of $(\text{PF})_{\text{max}}$ according to σ_{min} . The scatter of points around the averaged line is apparently due to the non-strict rectilinearity of the corresponding $\sigma S^2 - S$ dependences. When these dependencies are practically rectilinear, then the points fit well on the curve (compare Figs.1 and 2).

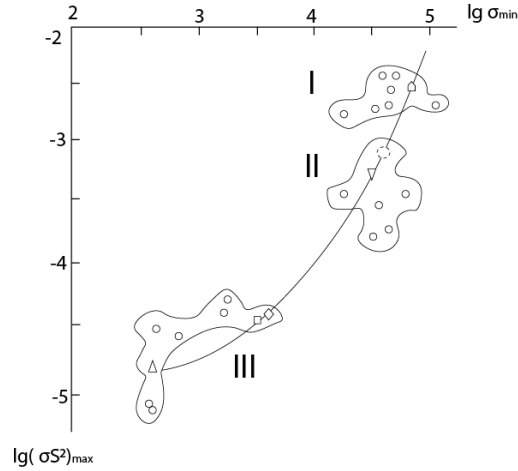


Fig. 2. Dependences $\lg(\sigma S^2)_{\text{max}} - \lg\sigma_{\text{min}}$. The coordinates of the points are calculated according to the data of following works: (sect.I) $\text{Si}_{0.7}\text{Ge}_{0.3}$ [17], SiGe , $\text{SiGeMo}_{0.2}$ [19], PbTe [21]; (sect.II) $\text{Sb}_{1.7}\text{Bi}_{0.4}\text{Te}_3$ [20], Bi_2Te_3 , $(\text{Bi}_{0.98}\text{Sn}_{0.02})_2\text{Te}_{2.7}\text{Se}_{0.3}$ [22], $\text{Si}_{0.68}\text{Ge}_{0.32}\text{Ga}$ [23], Ni_2CuCrFe [24]; (sect.III) $\text{Bi}_2\text{Sr}_2\text{Co}_{1.8}\text{O}_y$, $\text{Bi}_2\text{Sr}_{1.9}[\text{Sr}(\text{BO}_2)_2]_{0.1}\text{Co}_{1.8}\text{O}_y$ [18] (and the same thermoelectrics with different composition of components). Figurative points correspond to Fig.1: Δ - [19], \square - $\text{Si}_{0.72}\text{Ge}_{0.28}$, \diamond - [23], ∇ - [24], \circ - [24], \triangle - [19].

Figure 3 shows the temperature dependences of $\sigma S^2 - T$ and $S - \ln T$ for $\text{Si}_{0.72}\text{Ge}_{0.28}$ and $\text{Si}_{0.76}\text{Ge}_{0.24}$ (dependencies for other compositions have the same form). From this figure it is clear that these dependencies have a maximum at the same temperature ($\sim 1100\text{K}$).

It should be noted that for practically all other thermoelectrics considered above (and also for $\text{P-Si}_x\text{Ge}_{1-x}$), a rectilinear dependence of the Seebeck coefficient on the natural logarithm of temperature was observed (Fig.3). Therefore, for them the following formula was used [25,26]:

$$S = \frac{3}{2} \frac{k_B}{q_e} \ln T + C, \quad (1)$$

where C depends on the concentration and effective mass of charge carriers, as well as on the Debye temperature (k_B - Boltzmann's constant, q_e - elementary charge, T - absolute temperature)^(*). Figure 4(a) shows these dependences for $\text{P-Si}_x\text{Ge}_{1-x}$, and Figure 4(b) - for $\text{Sb}_{1.7}\text{Bi}_{0.4}\text{Te}_3$, $\text{Tl}_9\text{Sb}_{0.99}\text{Sn}_{0.1}\text{Te}_6$ [27] and $\text{SiGeMo}_{0.2}$. From Fig.4(a) it is clear that the experimental points form a practically single set with an

average overall slope $K \equiv \text{tg}\alpha \cong 1.122 \cdot 10^{-4}$. The slopes of the lines presented in Fig.4(b) are $\text{tg}\alpha \cong 1.324$, 1.475 and $1.050 \cdot 10^{-4}$, respectively. These slopes which approach to $K = \frac{3k_B}{2q_e} \cong 1.293 \cdot 10^{-4}$ with more or less accuracy.

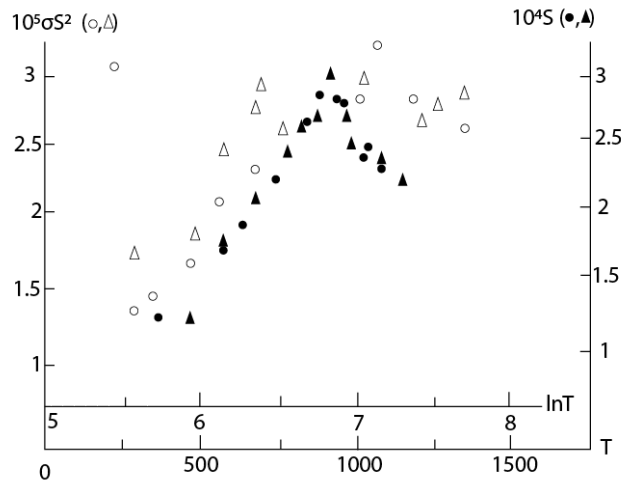
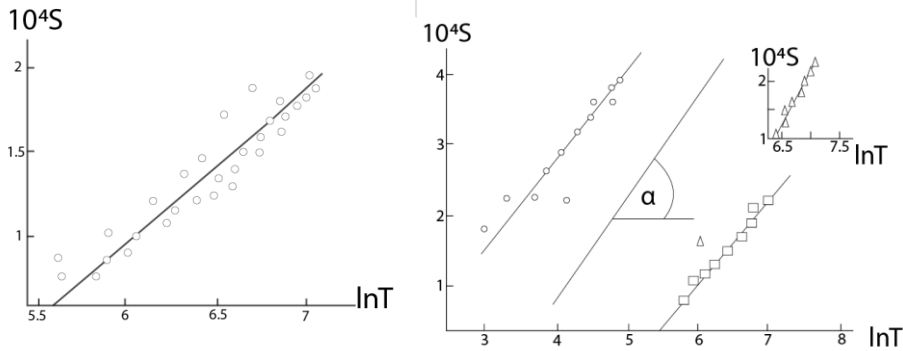


Fig. 3. Dependencies $\sigma S^2 - T$ and $S - \ln T$ for $\text{Si}_{0.72}\text{Ge}_{0.28}$ (o, Δ) and $\text{Si}_{0.76}\text{Ge}_{0.24}$ (\bullet , \blacktriangle).
 ($\ln 1100 \cong 7$, the scales are different on the abscissa axes).
 $[\sigma S^2] = \text{W/K}^2\text{m}$, $[S] = \text{V/K}$, $[T] = \text{K}$.



(a)(b)

Fig.4. Dependencies $S - \ln T$: (a) P-Si_xGe_{1-x} - $x=0.72, 0.76, 0.8$ at $n=3.2 \cdot 10^{26} \text{m}^{-3}$ and P-Si_{0.7}Ge_{0.3} at $n=2 \cdot 10^{26} \text{m}^{-3}$. The points belong to all values of x in Si_xGe_{1-x} (in most cases, the points for different x overlap each other);

(b) Sb_{1.7}Bi_{0.4}Te₃ (o), Tl₉Sb_{0.99}Sn_{0.1}Te₆ (Δ) and SiGeMo_{0.2} (□). A straight line without points was constructed at $\text{tg}\alpha \cong 1.293 \cdot 10^{-4}$ with arbitrarily taken $b=-4.4$. $[S]=\text{V/K}$.

Since the values of K do not coincide exactly with $\frac{3k_B}{2q_e}$, it is difficult to estimate the corresponding values of the constant A (see Footnote below) from the values of C calculated below. However, according to as yet unpublished data for P-Si_{0.7}Ge_{0.3}, the temperature dependence of mobility is described by the expression $\mu \cong \frac{1}{2} T^{-3/2}$, which indicates phonon scattering of charge carriers [28]. Figure 5 presents $\sigma S^2 - \sigma$ dependences for Si_{0.7}Ge_{0.3} and Tl₈Sn₂Te₆ [29]. The first is described by the empirical expression $\sigma S^2 \cong (108/\sigma) \cdot 1 \cdot 10^{-4}$, and the second: $\sigma S^2 \cong (37.5/\sigma) \cdot 4.5 \cdot 10^{-4}$. It should be noted that the second one is better described by the expression $\sigma S^2 \cong 6.728 \sigma^{-1.993}$. This is due to the fact that the $\sigma S^2 - S$ dependence for Tl₈Sn₂Te₆ is power law type and not rectilinear. And this is a more general case.

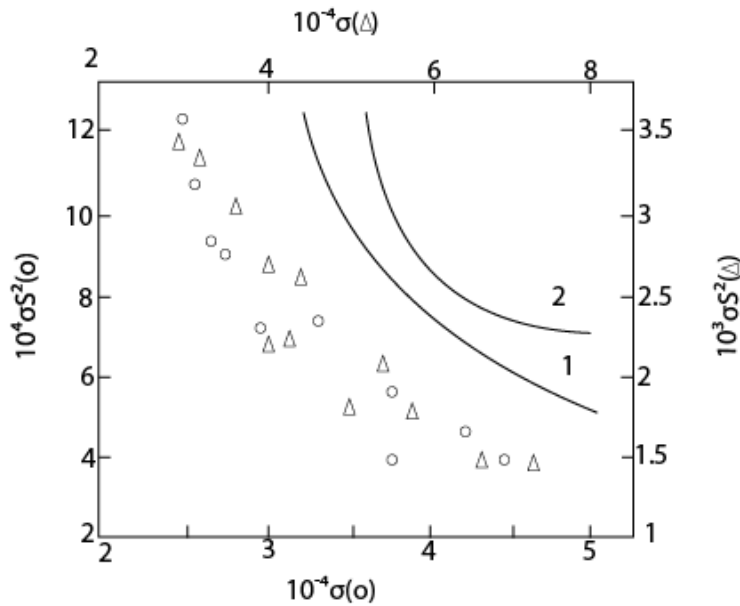
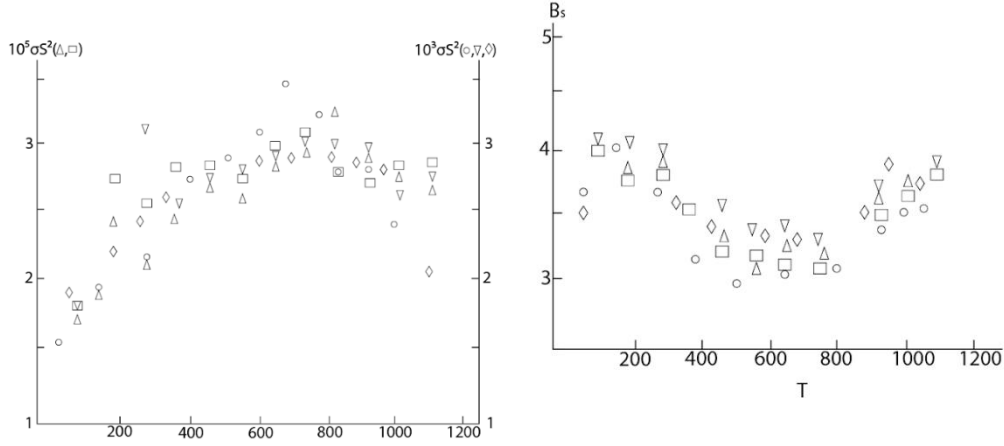


Fig. 5. Dependencies $\sigma S^2 - \sigma$: (o) - Tl₈Sn₂Te₆, (Δ) - Si_{0.7}Ge_{0.3}; lines without points- schematic graphs of functions $y=x^{-1/3}$ (1) and $y=ax^{-b}$, $b \neq -1/3$ (2). $[\sigma]=\text{Sim/m}$, $[\sigma S^2]=\text{W/K}^2$.

Temperature dependences of the power factor

Figure 6a shows the temperature dependences of the power factor for all samples N-Si_xGe_{1-x}, having the shape of a parabola with a negative coefficient at T^2 . Calculation of the scaled power factor ($B_S = \sigma S^2 / B_E$, where B_E is the electronic quality factor [30]) showed that its temperature dependence also has the shape of a parabola (but with a positive coefficient at T^2 (Fig.6b)). Presented in Fig.5 dependencies can be described by empirical expressions $\sigma S^2 = -1.67210^{-n} T^2 + 3.421 \cdot 10^{-n-3} T + 1.15 \cdot 10^{-n}$, where $n=3$ for Si_{0.7}Ge_{0.3}, Si_{0.8}Ge_{0.22}, Si_{0.83}Ge_{0.17} and $n=5$ for Si_{0.72}Ge_{0.28}, Si_{0.76}Ge_{0.24}; $B_S = 2.067 \cdot 10^{-6} T^2 - 3.905 \cdot 10^{-3} T + 4.9$. Both dependencies exhibit extremums at approximately the same temperature (1000-1100K). Since B_S depends

only on the Seebeck coefficient (it is given by the expression $B_S = \left[\frac{e^{S_r - 2}}{1 + e^{-5(S_r - 1)}} + \frac{\frac{3}{\pi^2} S_r}{1 + e^{5(S_r - 1)}} \right]$, where $S_r = \frac{q_e}{k_B} S$ is the reduced Seebeck coefficient), to estimate $(\sigma S^2)_{\max}$ can be used as σ_{\min} , and $(B_S)_{\min}$ (if the temperature dependencies of σS^2 and B_S are described by a quadratic equations).



(a)(b)

Fig. 6. Temperature dependences of σS^2 (a) and B_S (b) in $\text{Si}_x\text{Ge}_{1-x}$: $x=0.7$ (o), 0.72 (Δ), 0.76 (\square), 0.8 (\diamond) and 0.83 (∇).

$$[\sigma S^2] = \text{W/K}^2\text{m}, [T] = \text{K}.$$

Footnote:

(*) $C = \frac{k_B}{q_e} \left[A + \ln \frac{2(2\pi m^* k_B)^{3/2}}{(2\pi \hbar^3)^3 n} \right]$, where the constant A depends on the scattering mechanism and takes values from 2 to 4 (m^* and n – effective mass and concentration of charge carriers).

2. CONCLUSION

A method is proposed for determining the maximum power factor of $\text{Si}_x\text{Ge}_{1-x}$ alloys of different compositions and different conductivities. Other thermoelectrics are also considered based on literature data.

The dependences $\lg(\sigma S^2)_{\max} - \lg \sigma_{\min}$ for various thermoelectrics based on literature and our data in the corresponding interval of changes of variables are described by a single empirical expression $\lg(\sigma S^2)_{\max} \cong 0.583(\lg \sigma_{\min})^2 - 3.332 \lg \sigma_{\min}$.

The temperature dependence of the Seebeck coefficient described by the equation $S = \frac{3}{2} \frac{k_B}{q_e} \ln T + C$. This dependence has the same character as dependence $\sigma S^2 - T$ and have maximums around 1100K.

REFERENCES

1. Raag V. Dopant precipitation in silicon-germanium alloys, Proceedings of 7th Intersociety Energy Conversion Engineering Conference, San Diego, CA, USA, 25 September, 1972:445-4974.
2. Rowe DM. Recent developments in thermoelectric materials. *Applied Energy* 1986;24: 139-162.
3. Rosi FD. The research and development of silicon-germanium thermoelements for power generation. *MRS Online Proceedings Library*. 1991;234:3-26.
4. Basu R, Singh A. High temperature Si-Ge alloy towards thermoelectric applications. *Materials Today Physics*. 2021;21: 100468.
5. Cook B. Silicon-Germanium: The legacy lives on. *Energies*. 2022;15: 2957.
6. Schwinge C, Kühnel K, Emara J et al. Optimization of LPCVD phosphorous-doped SiGe thin films for CMOS-compatible thermoelectric applications. *Applied Physics Letters*. 2022;120:031903.
7. Big-Alabo A. Finite element modelling and optimization of Ge/SiGe super lattice based thermoelectric generators. *SN Applied Science*. 2021;3: 189.
8. Jang K, Kim Y, Park J et al. Electrical and structural characteristics of excimer laser-crystallized polycrystalline Si_{1-x}Ge_x thin-film transistors. *Materials*. 2019;12:1739.
9. Murata H, Nozawa K, Suzuki T et al. Si_{1-x}Ge_x anode synthesis on plastic films for flexible rechargeable batteries. *Scientific Reports*. 2022;12:13779.
10. Idda A, Ayat L, Dahbi N. Improving the performance of hydrogenated amorphous silicon solar cell using a-SiGe:Halloy. *Ovonic Research*. 2019;15:271-278.
11. Singh AK, Kumar M, Kumar D et al. Heterostructure silicon and germanium alloy based thin film solar cell efficiency analysis. *Engineering and Manufacturing*. 2020; 10:29-40.
12. Zimmerman H. SiGe photodetectors, in *Silicon Optoelectronic Integrated Circuits*, eds. Chun, K., Itoh, K., Lee, T.H. et al. Vienna, Austria, 2018: 1-435.
13. Aberl J, Brehm M, Fromherz J et al. SiGe quantum well infrared photodetectors on strained-silicon-on-insulator. *Optics Express*. 2019;27:32009-32018.
14. Koumoto K, Terasaki I, Funahashi R. Complex oxide materials for potential thermoelectric applications. *MRS Bulletin*. 2006;31: 206-210.

15. Ellis B L, Nazar L F. Sodium and sodium-ion energy storage batteries. *Current Opinion Solid State and Materials Science*. 2012;16: 168-177.
16. Bokuchava G. Physical-mechanical and electrophysical properties of polycrystalline silicon-germanium alloys, Thesis, Tbilisi, 2008: 1-135.
17. Nakhutsrishvili I, Adamia Z, Kakhniashvili G. Maximization of figure of merit of alloy $\text{Si}_x\text{Ge}_{1-x}$. *Materials Science Research and Reviews*. 2023;6: 918-922.
18. Barbakadze K, Bokuchava G, Isakadze Z et al. High temperature thermoelectric generator based on SiGe alloy. *Scientific Journal LEPL – Agmashenebeli National Defence Academy of Georgia*. 2022;47-50.
19. Kuzanyan A, Margiani N, Zhghamadze V et al. Effect of $\text{Sr}(\text{BO}_2)_2$ dopant on the power factor of $\text{Bi}_2\text{Sr}_2\text{Co}_{1.8}\text{O}_y$ thermoelectric. *Contemporary Physics*. 2021;56:146-249.
20. Li Y, Han J, Xiang Q et al. Enhancing thermoelectric properties of p-type SiGe by SiMo addition. *Materials Science: Materials in Electronics*. 2019;30:9163-9170.
21. Scheele M, Oeschler N, Veremchuk I et al. ZT enhancement in solution-grown $\text{Sb}_{2-x}\text{Bi}_x\text{Te}_{3-2x}$ nanoplatelets. *ASC Nano*. 2010;4: 4283-4291.
22. Sauerschnig P, Jood P, Ohta M. Improved high-temperature material stability and mechanical properties while maintaining a high figure of merit in nanostructured p-type PbTe-based thermoelectric elements. *Advanced Materials Technology*. 2023; 8:2201295.
23. Hedge G Ch, Prabhu A N, Chattopadhyay M K. Improved electrical conductivity and power factor in Sn and Se co-doped melt-grown Bi_2Te_3 single crystal. *Materials Science: Materials in Electronics*. 2021;32:24871-24888.
24. Omprakash M, Arivanandhan M, Koyama T et al. High power factor of Ga-doped compositionally homogeneous $\text{Si}_{0.68}\text{Ge}_{0.32}$ bulk crystal grown by the vertical temperature gradient freezing method. *Crystal Growth & Design*. 2015;15:1380-1388.
25. Kush L, Srivastava S, Jaiswal Y, Srivastava Y. Thermoelectric behaviour with high lattice thermal conductivity of Nickel base $\text{Ni}_2\text{CuCrFeAl}_x$ ($x = 0.5, 1.0, 1.5$ and 2.5) high entropy alloys. *Materials Research Express*. 2020; 7: 035704.
26. Tewari G C, Tripathi T S, Yamauchi H, Karppinen M. Thermoelectric properties of layered antiferromagnetic CuCrSe_2 . *Materials Chemistry and Physics*. 2014; 145: 156-161.
27. Tufail M, Shah W H, Shah U et al. Effects of Sn doping on the Seebeck coefficient and electrical conductivity of $\text{Tl}_9\text{Sb}_{1-x}\text{Sn}_x\text{Te}_6$ nanoparticles. *Chalcogenide Letters*. 2019;16: 175-184.
28. Alfaramavi K, Alzamil M A. Temperature-dependent scattering processes of n-type indium antimonide. *Optoelectronic Advanced Materials - Rapid Communications*. 2009; 3: 569-573.

29. Khan W M, Shah W H, Khan N et al. Effects on the seebeck co-efficient and electrical properties of $Tl_{10-x} A_x Te_6$ (A= Pb & Sn) in chalcogenide system. *Ovonic Research*. 2021;17: 201-208.

30. Zhang X, Bu Z, Shi X et al. Electronic quality factor for thermoelectrics. *Science Advances*. 2020;6:eabc0726.

UNDER PEER REVIEW